

# Space Weather: Forecasting the Sun-Earth Interaction.

C. Cid<sup>1</sup>

<sup>1</sup> SRG-Space Weather. Departamento de Física y Matemáticas. Universidad de Alcalá

## Abstract

Geomagnetic storms are considered as one of the natural hazards for modern society. Forecasting space weather is therefore a priority. However, scientific community is far to be able to provide accurate predictions from solar observations or even from interplanetary measurements. Even more, the quantification of the severity of the disturbance at the terrestrial surface by scientific community using global indices as Dst cannot be considered as the best proxy to give account of the damage in utilities, and local disturbances appear as the relevant proxy. Detailed studies of individual events show that one of the main reasons for the poor prediction capability is the lack of understanding of the complete event in all of the stages of its Sun-to-Earth passage. Using some examples, this paper evidences that a multi-disciplinary approach with interplanetary medium as a key-point is a fast track for truthful space weather forecasts.

## 1 Introduction

Since Carrington [1] suggested a cause-effect relationship between a moderate but very marked magnetic disturbance at Kew observatory and white light flaring, a lot of progress has been made in relating the cause of disturbances in the Earth and the near-Earth space environment with solar activity. For many years, this scientific progress was mainly made in the pursuit of knowledge, and remained completely separated from the effects of solar activity on technology. However, since the Hydro-Quebec system blackout in March 1989 leaving 6 million people without power for 9 hours, the vulnerability of technology to solar activity has become an issue, especially because thousands of satellite tracking problems were also reported during that event.

Nowadays technology is even more vulnerable to space weather than in 1989, but data sets have improved since that time in quality and in temporal and spatial resolution (Fig. 1). As an example, many everyday tasks in society depend on Global Navigation Systems

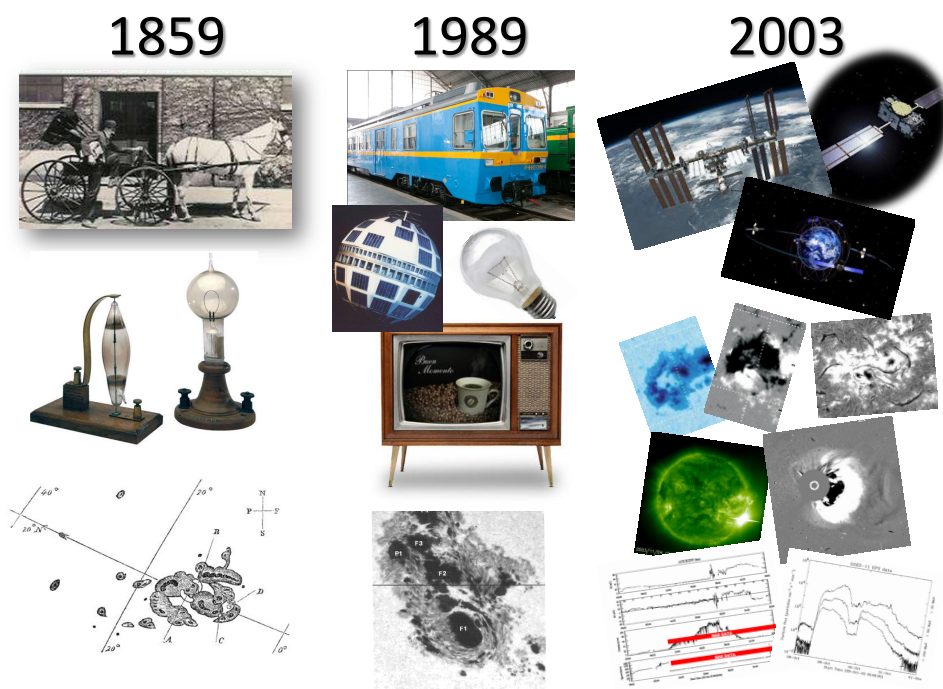


Figure 1: The Figure illustrates the state-of-the-art technology and solar observations at the epoch of the three major space weather events when large damages were reported: the Carrington event in October 1859, the Quebec blackout in March 1989, and the South Africa power outage in October 2003.

nowadays. Since 1995 when GPS became operational, it is not only supporting communications systems, but also power grid systems, transportation systems and banking operations. Space weather effects on GPS have been recognized since 2000 when scintillation was shown to cause loss of lock on GPS signals during ionospheric storms at mid-latitudes.

The October 2003 storm, which threatened the electrical grid in South Africa and Sweden, cannot be missed in the short list of historical records of extreme geomagnetic storms due to its consequences for society. After the South Africa blackout, power companies located at mid-latitudes are now also aware of space weather.

Some recently detected problems onboard satellites and have questioned seriously our capability to predict such space weather events. Among these, it is the example of Intel-sats five-year-old Galaxy 15 satellite, which stopped responding to commands in early April 2010 despite the fact that solar activity and solar wind features indicated that only minor disturbances occurred.

But space weather is not as simple as observing a large flare and then recording a terrestrial disturbance. Nowadays large terrestrial disturbances are statistically related to the closest in time large flare and/or fast halo CME within the correct time window (flare effects can appear in the Earth in minutes, whereas CMEs take normally 2 to 4 days to

arrive). But taking flares as the only precursors without considering other features may be insufficient from the geoeffectiveness point of view, since more than 80 % of CMEs are not associated with a large flare ([12]).

Detailed studies of individual events show that one of the main reasons for the poor prediction capability is the lack of understanding of the complete event in all of the stages of its Sun-to-Earth passage. The available data can be much better exploited than has hitherto been achieved through using case-studies. To this end, data sets measured during severe disturbances must be analysed from the terrestrial surface back to their origin on the solar source. Moreover, consequences for space assets, ground infrastructures and navigation services in specific scenarios must be analysed, not as a final stage, but rather as the main focus. Furthermore, different kinds of vulnerability should be considered separately.

This paper is focused on geomagnetic disturbances, which are the cause of damages in ground infrastructures. Therefore, light and high energetic particles coming from solar activity are not an issue for this paper, but only solar wind disturbances reaching the Earth at least one day after the solar ejection. The interplanetary magnetic field and solar wind plasma interact with the terrestrial magnetosphere generating currents that flow into the magnetosphere and down into the ionosphere. The most intense currents ionospheric are associated with the aurora and confined in what it is called the auroral electrojet. The magnetic field produced by these currents is seen on the ground as a magnetic disturbance which may produce damages in infrastructures based on long wires.

## 2 The cause of geomagnetic disturbances

Cid et al. [5] noted that extreme geomagnetic disturbances present a marked local character. Nevertheless, these disturbances have been considered for ages as planetary disturbances and geomagnetic indices have been established for their analysis. In this way, the Dst index, which measures the deviation in the horizontal component of geomagnetic field at the ground at four low latitude observatories widely distributed in longitude (Hermanus, Kakioka, Honolulu, and San Juan), is used to define the term geomagnetic storm and its intensity ([8], [7]). According to [8] an intense geomagnetic storm appears as a decrease of the Dst index below the threshold value of -100 nT.

Large decreases of Dst index have been related with several forms of solar activity, but CMEs reaching the Earth are considered as the most probable solar trigger of intense geomagnetic storms ([9], [10], [8]). This fact is based on assuming that the energy transfer mechanism from solar wind to the magnetosphere is magnetic reconnection between the interplanetary and the Earth's magnetic field. The interplanetary dawn-dusk electric field given by  $VB_z$  drives the process [6], being  $B_z$  the southern interplanetary magnetic field and  $V$  the solar wind velocity. In this scenario, magnetic clouds, which are the interplanetary counterpart of CMEs, appear as the solar wind disturbances that present the most intense and long southern interplanetary magnetic field, and also the largest values of solar wind velocity. As a consequence, CMEs reaching the Earth are expected to be the most geoeffective transients. In this way, studies relating the CMEs passage to drops in the Dst index just

based on a reasonable delay between both phenomena found a theoretical explanation.

The interpretation of full-halo CMEs as a 2-D projection of solar material propagating approximately towards or away from the observer in the interplanetary space by [11], guided to consider full-halo CMEs with on-disk signatures as the most probable source of geomagnetic disturbances. Nowadays it is well known that other propagation directions are consistent with full-halo CMEs and to find out from solar images when the material is approaching to the Earth is not an easy task [4]. An approach to solve the problem was done trying to restrict the solar source location of the full-halo CME to those regions close to solar central meridian, but the position of the active region (AR) on the solar disk is not a trustworthy factor when determining possible geoeffectiveness: an eruptive active region located in the central meridian is easy to identify as a main precursor, but eruptions from active regions can be also geoeffective when located close to the limb [3].

Far from statistical analysis, [3], [14], [2] are examples of carefully analysis of selected geomagnetic storms along the whole Sun-to-Earth chain. These analyses provided two major findings. On one side, they concluded that interaction between solar ejections is the base of severe disturbance. In this interaction, solar coronal holes might play a major role. On the other hand, they also conclude that results from statistical studies based on a reasonable delay between solar ejection and terrestrial disturbance are not reliable.

The geomagnetic storm on 11 March 2011 (Fig. 2) can be considered also as an example of this last relevant result. A full-halo CME appeared at C2/LASCO at 20:00 UT on 7 March 2011. From the height-time plot, the LASCO team estimated a velocity on the plane of the sky of  $2125 \text{ km s}^{-1}$ . The CME was related to an M3.7 flare at 19:43 UT from AR 11164 located in the NorthWest (see top left panel in Fig. 2). In an statistical study, the halo CME and the associated flare would be considered as the solar triggers of the decrease of SYM-H index (which can be considered as a high temporal resolution Dst index) starting on 10 March and reaching its peak value on 11 March (see bottom right panel in Fig. 2). However, a careful analysis of all the stages from the Sun to the Earth reveals that this association is wrong, as it will be shown below.

The shadowed area in right panel of Figure 2 corresponds to the whole geomagnetic storm event, according to the SYM-H index. Before this interval all solar wind parameters show quiet conditions. After the shadowed area, a very low magnetic field feature appears with enhanced solar wind velocity and temperature, which are typical features of a fast stream arising from a solar coronal hole. Between the white background areas, the shadowed area encloses an interaction region between the slow and fast wind where magnetic field is enhanced and density is low while velocity is gradually increasing. It is this interaction region, and therefore the coronal hole, the final trigger of this geomagnetic storm, and no sign of any CME can be guessed in the interplanetary medium data.

Interplanetary medium analysis guides us to revise solar observations and to finally discover that the full fast halo CME from AR11164 never reached the Earth. The definitive conclusion is supported from the analysis of Proba2/SWAP images, where a UV wave appears at 19:42 UT showing clearly that the CME was directed towards the North West of the Sun.

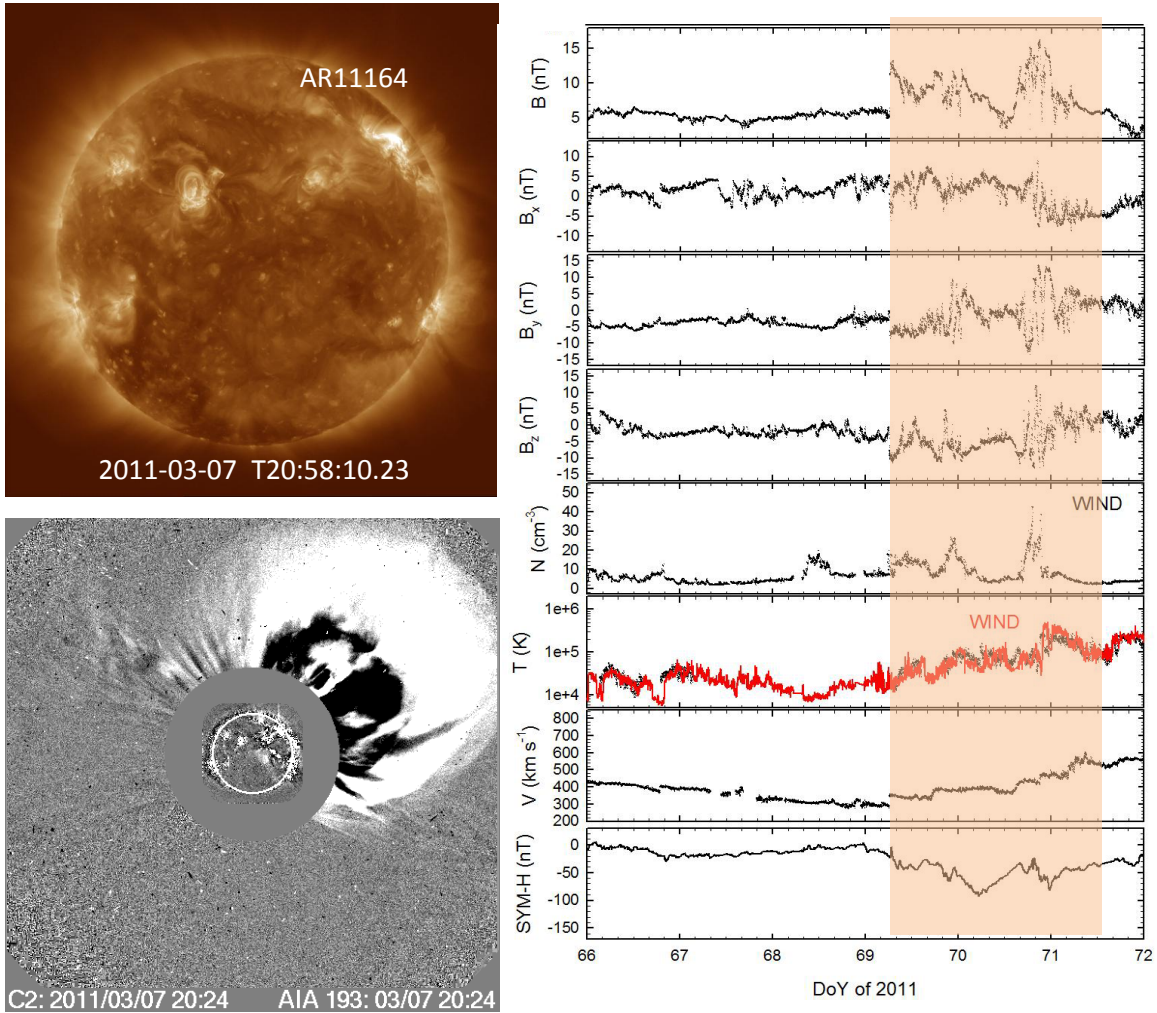


Figure 2: Top left panel shows solar disk on AIA 193 on 7 March 2011 at 20:58:10.23 UT with the AR11164 in the North West. Bottom left panel shows a composition of C2/LASCO and AIA 193 images (Universal time is indicated in each image) with a initial stage of the full-halo CME described in the text. Right panel presents solar wind measurements from 7 to 13 March 2011 (DoY 66-72) and SYM-H index as a proxy of geomagnetic activity. From top to bottom the panels show magnetic field strenght and GSM components and solar wind plasma parameters: density, temperature and velocity. Shadowed area corresponds to an interaction region between slow and fast solar wind.

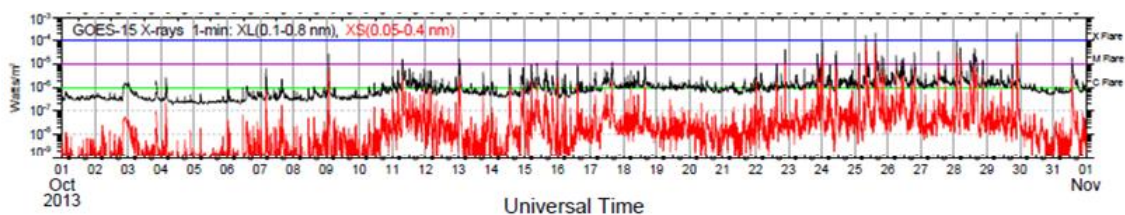


Figure 3: The Figure shows the X-ray flux from GOES-15 satellite in channels 0.1-0.8 nm and 0.05-0.4 nm in October 2013.

### 3 Breaking down paradigms around flares and CMEs

Close to the peak of Solar Cycle 24th, October 2013 was a month with major flaring activity. Figure 3, which shows the X-ray flux from GOES-15 satellite, shows a large activity during the last third of the month and also some activity on the second third. Space weather alerts from NOAA include X-flare events with X-ray flux exceeding  $5 \times 10^{-5} \text{ W m}^{-2}$  in channel 0.1-0.8 nm, i.e. larger than M5. Five flare events should therefore be notified in October 2013, all of them from 24 to 29 (Table 1). Some of the flare events were associated with CMEs.

SOHO/LASCO halo CME catalogue at [http://cdaw.gsfc.nasa.gov/CME\\_list/halo/halo.html](http://cdaw.gsfc.nasa.gov/CME_list/halo/halo.html) includes eleven events observed during October 2013 (Table 1). Three of them present an apparent speed larger than  $1000 \text{ km s}^{-1}$  and five of them were related to larger than M5 flares.

Table 1: Major Flares (larger than M5.0) and full-halo CMEs in October 2013

Day	Flare Time (hh:mm)	AR No.	Flare/ejection location	Flare Imp.	CME time (hh:mm)	Apparent Speed ( $\text{km s}^{-1}$ )
05			S22E118		07:09	964
06			S16W13		14:43	567
11			N21E103		07:24	1200
22		11875	N04W01		21:48	459
24	00:21	11877	S10E08	M9.3	01:25	399
25	07:53	11882	S08E73	X1.7	08:12	587
25	14:51	11882	S06E69	X2.1	15:12	1081
26		11882	S05E58		11:24	796
28	01:41	11875	N04W66	X1.0	02:24	695
28					15:36	812
29	21:42	11875	N05W89	X2.3	22:00	1001

Regarding geomagnetic activity, the Dst index from Kyoto WDC (<http://wdc.kugi.kyoto-u.ac.jp/dst/dir/>) shows four disturbed periods in October 2013 starting on days 2, 8, 14 and

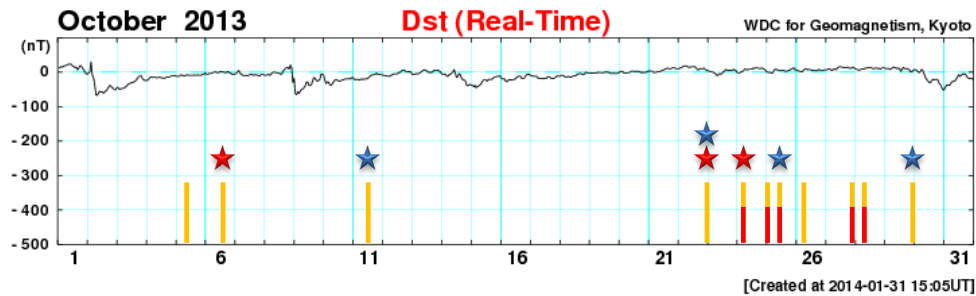


Figure 4: The Figure shows Dst index from Kyoto WDC in October 2013. Some symbols (coloured bars and stars) have been inserted in the figure to show solar activity at that time. Vertical yellow bars corresponds to full-halo CMEs and vertical red bars indicate X-class flares larger than M5. A red star on the top indicates apparent velocity larger than  $1000 \text{ km s}^{-1}$  for the CME and a blue star indicates flare/ejection location between E15 and W15.

30 (Fig. 4). Figure 4 displays also some symbols related to solar activity at that time: vertical yellow bars corresponds to full-halo CMEs and vertical red bars indicate X-class flares larger than M5. A red star on the top indicate apparent velocity larger than  $1000 \text{ km s}^{-1}$  for the CME and a blue star indicate flare/ejection location between E15 and W15, i.e., close to central solar meridian.

Just a glance to Figure 4 is enough to break down the old paradigm relating large flares, fast halo CMEs and geomagnetic storms, even if the eruption is close to solar central meridian and even if velocity is large. But a detailed analysis including the interplanetary medium data is needed in order to provide solid scientific-based reasons on the true solar triggers of these terrestrial disturbances.

A careful analysis of the geomagnetic storm starting on October 2nd reveals that it is related to a large solar filament eruption on 29 September. The smooth eruption, which passed without any previous flare, formed after a two-ribbon C flare and a halo CME was ejected towards Earth ([?]).

Although with some data gaps, interplanetary data from 8 to 11 October show clearly that the geomagnetic disturbance starting on October 8th is related to a solar ejection. The sudden commencement of the storm is indeed related to the forward interplanetary shock missed in the two hours gap of October 8. However, it is reasonable to guess it as a consequence of the jump from a solar wind velocity close to  $300 \text{ km s}^{-1}$  during this day until about 17 UT to above  $450 \text{ km s}^{-1}$  just after the data gap and reaching more than  $600 \text{ km s}^{-1}$  before the end of the day and peaking at a value slightly above  $650 \text{ km s}^{-1}$ . This last velocity value, which is between the linear speed ( $567 \text{ km s}^{-1}$ ) and 2nd order speed at 20 solar radii ( $822 \text{ km s}^{-1}$ ) from LASCO catalogue, is consistent with the time of travelling from the Sun to the Earth. Although this fact makes the full-halo CME a highly probable source for the geomagnetic disturbance starting on October 8th, a deeper analysis of solar images from different sources and solar wind parameters is needed to be conclusive. This analysis will explain why the magnetic field strength reaches almost 40 nT and solar wind density

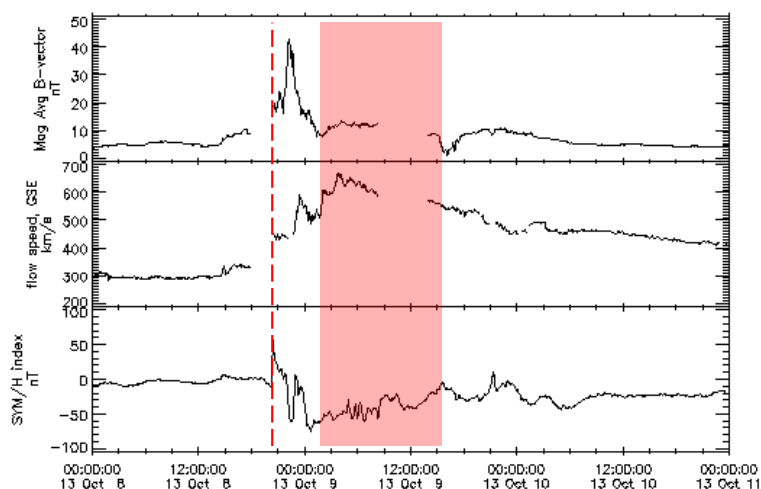


Figure 5: From top to bottom, this Figure shows interplanetary magnetic field intensity, solar wind velocity and SYM-H magnetic index 5-minute resolution data during the period 8 to 11 October 2013. OMNI solar wind data are time-shifted to the nose of the Earth's bow shock. Dashed line corresponds to the sudden commencement of the geomagnetic storm. Shaded area corresponds to the interplanetary counterpart of a CME.

almost 60 particles per  $\text{cm}^{-3}$ , as those values suggest that some kind of interaction between different ejections took place at some place between the Sun and the Earth.

The analysis of solar wind parameters during the disturbance on 14-15 October, reveals that it is clearly related to the interaction region between slow solar wind and fast one emanating from a coronal hole which passed the solar central meridian on 10-11 October 2013 (Fig. 6). No signature of eruption can be guessed in solar wind data from ACE spacecraft for this event.

Interplanetary data from 24 October to the end of the month show quiet to unsettled conditions with solar wind velocity between 300 to 450  $\text{km s}^{-1}$ . The interplanetary magnetic field is enhanced up to 12 nT and largely fluctuating during 30-31 October, when solar velocity is large, with no clear signature of any counterpart of a CME. As a result, we conclude that no flare or CME from the last third of October reached the Earth. Checking solar disk images from SDO/AIA, several coronal holes can be observed, which are the cause of the last geomagnetic disturbance observed in October 2013.

## 4 Summary and conclusions

Sun-Earth interaction analysis during October 2013 reveals that space weather is a young discipline that still needs to address many open issues in the upcoming years. In this scenario, interplanetary physics appears as a key issue to properly relate solar cause and terrestrial effects. Moreover, scientific community should also be aware of the local character of the

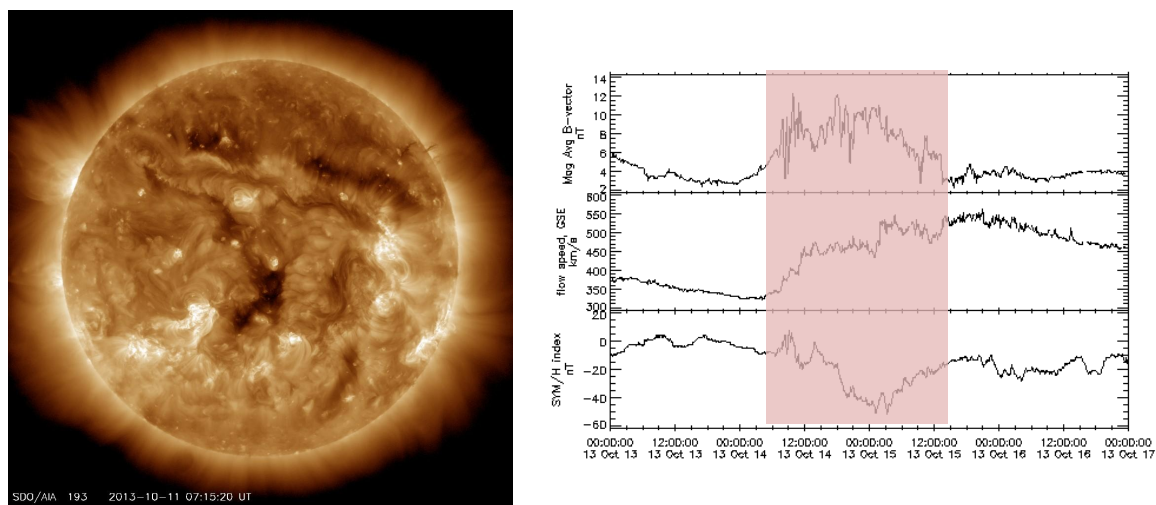


Figure 6: Left panel: Solar disk image on 11 October 2013 at 07:15:20 UT in 193 A from SDO/AIA. Right panel (from top to bottom): Interplanetary magnetic field strength, solar wind velocity and SYM-H index 5-minute resolution data during the period 13-17 October 2013. OMNI solar wind data are time-shifted to the nose of the Earth's bow shock. Shadowed area corresponds to the interaction region between slow solar wind and the fast stream.

terrestrial disturbances, as this is a major issue for the potential users of any space weather service. Increasing the interaction between research on different disciplines involved in space weather and aware potential users is on progress.

## Acknowledgments

We want to acknowledge SDO/AIA, SWAP/Proba2 and ACE/SWEPAM and ACE/MAG Data Science Centers and Teams, also to GOES and LASCO/SOHO teams. Also we acknowledge data use from WDC from Geomagnetism, Kyoto, CDAweb Space Physics Data Facility at Goddard Space Flight Center, and NOAA National Geophysical Data Center. This work has been supported by the Spanish MINECO under the project AYA2013-47735-P.

## References

- [1] Carrington, R. C. 1859. *MNRAS*, 439, 13
- [2] Cerrato, Y., et al. 2012, *J. Atm. Sol. Terr. Phys.*, 80, 111
- [3] Cid, C. et al. 2012, *J. Geophys. Res.*, 117, A11102, doi:10.1029/2012JA017536
- [4] Cid, C. et al. 2013, *Proc. IAU S300*, 285
- [5] Cid, C., et al. 2014, *J. Space Weather Space Clim.* 4, A28, doi: 10.1051/swsc/2014026
- [6] Dungey, J. W. 1961, *Phys. Res. Lett.*, 6, 47
- [7] Echer, E., Gonzalez, W. D., & Tsurutani B. T. 2008, *Geophys. Res. Lett.*, 35, L06S03

- [8] Gonzalez, W. D., et al. 1994, *J. Geophys. Res.*, 99, 5771
- [9] Gonzalez, & W.D. Tsurutani 1987, *Plan. Sp. Sci.*, 35, 1101
- [10] Gosling, J. T., et al. 1991, *J. Geophys. Res.*, 96, 7831
- [11] Howard, R.A., et al. 2007, *ApJ*, 263, L101
- [12] Linker, J. A., et al. 2003, in *Solar Wind Ten*, vol. 679 *AIP Conf. Ser.*, 703
- [13] Palacios J., et al. 2015, *A&A*, under review
- [14] Rodriguez, L., et al. 2009, *Sp. Weather*, 7, S06003